


Article

# Adsorptive Removal Behavior of Pb (II) and Cr (VI) Pollutants from an Aqueous Environment onto Polyaniline-Modified MIL100(Fe)

Asghar Azizi <sup>1</sup>, Mojtaba Forghani <sup>1</sup>, Leila Asadi Kafshgari <sup>2</sup> and Ahmad Hassanzadeh <sup>3,4,\*</sup> 

<sup>1</sup> Faculty of Mining Engineering, Petroleum and Geophysics, Shahrood University of Technology, Shahrood 36199-95161, Iran

<sup>2</sup> Department of Chemical Engineering, Babol Noshirvani University of Technology, Shariati Ave., Babol 47148-73113, Iran

<sup>3</sup> Department of Geoscience and Petroleum, Faculty of Engineering, Norwegian University of Science and Technology, 7491 Trondheim, Norway

<sup>4</sup> Maelgwyn Mineral Services Ltd., Ty Maelgwyn, 1A Gower Road, Cathays, Cardiff CF24 4PA, UK

\* Correspondence: ahmad.hassanzadeh@ntnu.no or ahassanzadeh@maelgwyn.com; Tel.: +49-176-2066-6711

**Abstract:** The present work introduces a new sorbent, so-called PANI/MIL100(Fe), for removing Pb (II) and Cr (VI) from wastewater. The successful preparation of PANI/MIL100(Fe) was verified via Fourier-transform infrared spectroscopy (FT-IR), X-ray powder diffraction (XRD), scanning electron microscopy (SEM), and Brunauer–Emmett–Teller (BET) characterizations. This adsorptive material showed a microporous structure with surface area magnitudes of up to 261.29 m<sup>2</sup>/g, a total pore volume of 0.2124 cm<sup>3</sup>/g, and a pore size distribution of around 1.2 nm. The maximum adsorption capacities of PANI/MIL100(Fe) for Cr (VI) (pH = 2) and Pb (II) (pH = 6) were obtained as 72.37 and 81.76 mg/g, respectively. The isotherm modeling assessments illustrated that the sorption of Pb (II) and Cr (VI) was consistent with the Sips model ( $R^2 > 0.99$ ), while the adsorption kinetics were suited to a pseudo-second-order model ( $R^2 > 0.95$ ). Thermodynamic studies of both metal ions demonstrated the spontaneous and endothermic nature of the process. The reusability of the PANI/MIL100(Fe) indicated promising adsorption properties for Pb (II) and Cr (VI) up to three cycles. Moreover, the XRD and FT-IR spectroscopy results after adsorption/desorption showed excellent stability of the adsorbent and physisorption mechanism, wherein electrons were exchanged between the PANI/MIL-100(Fe) and Pb (II) and Cr (VI). Finally, the findings suggested that PANI/MIL100(Fe) can be considered an efficient and environmentally friendly adsorbent to remove Pb (II) and Cr (VI) from wastewater.

**Keywords:** PANI/MIL100(Fe); hydrothermal process; adsorption characteristics; Pb (II); Cr (VI)



**Citation:** Azizi, A.; Forghani, M.; Kafshgari, L.A.; Hassanzadeh, A. Adsorptive Removal Behavior of Pb (II) and Cr (VI) Pollutants from an Aqueous Environment onto Polyaniline-Modified MIL100(Fe). *Minerals* **2023**, *13*, 299. <https://doi.org/10.3390/min13030299>

Academic Editor: Chiharu Tokoro

Received: 15 January 2023

Revised: 8 February 2023

Accepted: 14 February 2023

Published: 21 February 2023



**Copyright:** © 2023 by the authors. Licensee MDPI, Basel, Switzerland. This article is an open access article distributed under the terms and conditions of the Creative Commons Attribution (CC BY) license (<https://creativecommons.org/licenses/by/4.0/>).

## 1. Introduction

Nowadays, water-soluble metal ions in wastewater treatment have attracted considerable attention. A substantial amount of wastewater with toxic heavy metals is directly or indirectly discharged into the environment, causing heavy metallic ions to be accumulated in ecosystems and causing intensive environmental problems. Heavy metal pollution can harm the brain, kidneys, nervous system, and other organs, even at low concentrations [1].

Cr (VI) and Pb (II) are common heavy metal contaminants with a high degree of toxicity, stability, and mobility in industries, namely battery manufacturing, metallurgy, metal plating, mining, fertilizers, pesticides, and paper industries [1,2]. Chromium in the food chain can lead to changes in human physiology and accordingly cause serious health problems including simple skin irritation and lung cancer. Lead can create intensive dysfunction in the kidneys, liver, and reproductive system [1]. Generally, unlike organic pollutants, which are chemically oxidized or biodegraded, heavy metal contaminants with high toxicity are usually not easily degradable, and their treatment is difficult. Therefore,

an appropriate strategy is needed to develop a new system for tracing the metal ions and their efficient removal from liquid phases.

At present, conventional technologies used for removing chromium and lead ions from aqueous solutions mainly consist of chemical precipitation, membrane filtration, electrochemistry, biological treatment, ion exchange, and adsorption [3–7]. The adsorption method is a technique for removing lead and chromium ions in water via ion exchange, complexation, and adsorption by an adsorbent. This method has the advantages of low cost, low energy consumption, high efficiency, lower environmental impacts, and better regeneration capability. Therefore, the adsorption technology has broad application prospects in dealing with metal pollution in water [8]. This process depends on a lot of factors, one of the most important of which is pH, because it can alter both the surface charge characteristics of the adsorbent and metal ion species distribution in an aqueous solution [9]. For example, Rodríguez et al. [10] examined the removal of heavy metals (Fe, Cu, Zn, and Al) from acid mine drainage water in the mining areas of the Huelva province, Spain, and reported that at a pH of 3.5, most of the iron was removed while Zn and Cu were partially removed. Moreover, at a pH of 5.5, the removal of all the above metals increased considerably.

Metal–organic framework (MOF) material is a porous material that has been developed rapidly recently. In 1995, Yaghi and Li [11] synthesized MOF materials for the first time. MOFs exhibit excellent performance for the adsorption of ions from aqueous media [12–15], gas storage and separation [16], sensors [17], photochemical properties [18], catalysis [19], and drug delivery [20], owing to their high porosity and surface areas, fascinating topology structures, abundant unsaturated sites, diverse post-modification potentials, adjustable hole size, and tailored chemistry. MOFs displayed excellent performance on the adsorption of intended pollutants owing to the presence of coordinatively saturated or unsaturated metal sites [1]. In the structures of MOFs, metal coordination centers are linked by multi-dentate organic ligands to produce three-dimensional extensible networks to create high porosity.

MIL100(Fe), as an iron-trimesic MOF, is a promising agent for water purification because of (I) the little toxicity of Fe ions, (II) light and low-cost accessibility of synthesis precursors, (III) powerful hydrolytic stability of coordinative structure contributed by strong Lewis acidity of trivalent iron, (IV) the simplicity of synthesis approaches and their environmental aspects, and (V) great unsaturated functional groups of organic linkers' potential for adsorption of metal ions [21].

A high number of systematic research works have been carried out on the adsorptive removal of heavy metal ions using MOFs. For instance, Rahimi utilized the Cu-based MOF for the sorption of Pb (II) and Cd (II) and reported that the sorption capacity was considerably greater than that of mordenite zeolite (MOR) or graphene oxide (GO) [22]. Zhongmin et al. [8] prepared magnetic orderly mesoporous  $\alpha$ -Fe<sub>2</sub>O<sub>3</sub> nanoclusters using thermal decomposition of MIL-100(Fe) to examine the sorption attributes on As (III) and As (V). Their findings demonstrated that the highest sorption capacity of As (III) and As (V) was found to be 109.89 and 181.82 mg/g after 30 min, respectively. Moreover, some conductive polymers such as polypyrrole (PPy) and polyaniline (PANI) were adopted to modify the MOFs to promote conductivity and enhance the separation, due to their low cost, non-toxic, high electrical, and optical attributes.

Polyaniline (PANI) is one of the most important nanostructured polymers with  $\pi$ – $\pi$  conjugated structures, which in recent years attracted great attention from researchers owing to its low cost of monomer, high electrical conductivity, superior environmental stability, simple synthesis, and polar functional groups [23]. PANI has also demonstrated an excellent sorption performance to remove heavy metal contaminants from wastewaters because of imine functionality, high value of amine (–NH) and marvelous groups in the polymer chains, and good redox properties, as well as a large surface area to volume ratio [24]. Karthik et al. [25] evaluated the polyaniline-grafted chitosan particles for adsorption of Pb (II) and Cd (II) in a batch system. Their results showed that the highest sorption capacity achieved was 16.07 and 14.33 mg/g for Pb (II) and Cd (II), respectively,

based on the Langmuir isotherm. Meanwhile, suitable pH was 6 for high sorption of Pb (II) and Cd (II) ions. A large number of studies have been conducted to modify PANI with many materials to increase the adsorption capacity and make them more processable in the treatment techniques of water [26]. Composite materials demonstrate superior thermal and chemical stabilities, sorption capacities, granulometric properties, and also have higher selectivity in the removal of heavy metal ions compared to pure inorganic and organic materials [27].

This study aims to combine MOF materials with polyaniline in a certain way to ensure the improvement of adsorption capacity. The catalytic and photocatalytic behaviors of PANI/MIL100(Fe) composite have been examined in the various reactions, but its potential on the sorption performance of hazardous ions was barely reported. Thus, in this research, the effects of PANI/MIL100(Fe) on Pb (II) and Cr (VI) adsorption were systematically investigated. In this regard, firstly, PANI/MIL100(Fe) was synthesized under ambient conditions and characterized by elemental analysis, XRD, FESEM, FT-IR spectroscopy, and BET. Then, the effects of the solution's pH, sorption isotherm, kinetic, and thermodynamic properties were addressed to detect the optimum conditions for the removal of Cr (VI) and Pb (II). Moreover, the XRD and FT-IR spectroscopies after adsorption/desorption were used to study the adsorbent stability and mechanism of the reaction.

## 2. Materials and Methods

### 2.1. Chemicals

Iron (III) nitrate nonahydrate  $\geq 99\%$  ( $\text{Fe}(\text{NO}_3)_3 \cdot 9\text{H}_2\text{O}$ ), 1,3,5-benzenetricarboxylic acid (TMA;  $\text{H}_3\text{BTC}$ , 98%), hydrogen fluoride (HF, 48.0%), nitric acid ( $\text{HNO}_3$ , 65%–68%), hydrochloric acid (HCl, Merck), ammonium peroxydisulfate (APS), and aniline were all purchased from Merck (Darmstadt, Germany). Aniline monomer was distilled under a reduced pressure. All chemical reagents used in this study were employed without purification. In this study, potassium bichromate ( $\text{K}_2\text{Cr}_2\text{O}_7$ ) and lead nitrate ( $\text{Pb}(\text{NO}_3)_2$ ) were utilized for providing the stock solutions.

### 2.2. Fabricate of PANI/MIL-100(Fe) Composite

The MIL-100(Fe) used in this research was fabricated by the improved procedure according to the literature [1]. Concisely, 8.0 Fe: 5.36 TMA: 24 HF: 4.8  $\text{HNO}_3$ : 2240  $\text{H}_2\text{O}$  were first blended and sealed in a 60 mL Teflon-lined autoclave and conducted hydrothermal reaction at 160 °C for five days. Then, the synthesized composition was purified by solvent extraction route employing hot ethanol/water. The obtained powders were filtered, washed via distilled/deionized (DD) water, and dried under electric oven at 60 °C for 12 h (Figure 1a) [28].

The PANI/MIL-100(Fe) composite was prepared through an in situ chemical oxidative polymerization monomer of aniline with the help of oxidizing agent of ammonium peroxydisulfate (Figure 1b). First, 0.3 g of MIL-100(Fe) was poured into 80 mL of DD water and ultrasonicated for 20 min. After this, aniline monomer (0.0644 M), HCl (1 M), and 50 mL of DD water were poured into dispersion. After 20 min, APS (0.0208 M) was poured slowly into the reaction mixture with continuous stirring at 0–5 °C. Within a short time, the color of the mixture changed to greenish black. The polymerization process was conducted in an ice bath for almost 24 h. After this process, the powder was purified by centrifugation (6000 rpm) using the reaction solvent to pull out any impurities. Ultimately, the resultant composite was dried at 50 °C [29].

### 2.3. Characterization Techniques

The X-ray diffraction (XRD) patterns were assessed using an X'Pert MPD X-ray diffractometer (Philips PANalytical, Almelo, The Netherlands) at  $\text{Cu K}\alpha$  irradiation. A Bruker Tensor 27 FT-IR spectrometer (Bruker, Billerica, MA, USA) was applied to record Fourier-transform infrared spectroscopy (FT-IR) of the materials. The surface morphology of composite was examined utilizing Zeiss-EM10C Transmission Electron Microscope (TEM,

Oberkochen, Germany) with an accelerating voltage of 80 kV. The Brunauer–Emmett–Teller (BET) analyses were used for determining the pore size distributions and specific surface areas via a N<sub>2</sub> adsorption/desorption instrument (Belsorp-mini II, Osaka, Japan) technique. The zeta potential was measured using a microprocessor pH meter (pH211, Hanna Instruments Inc., Woonsocket, RI, USA).

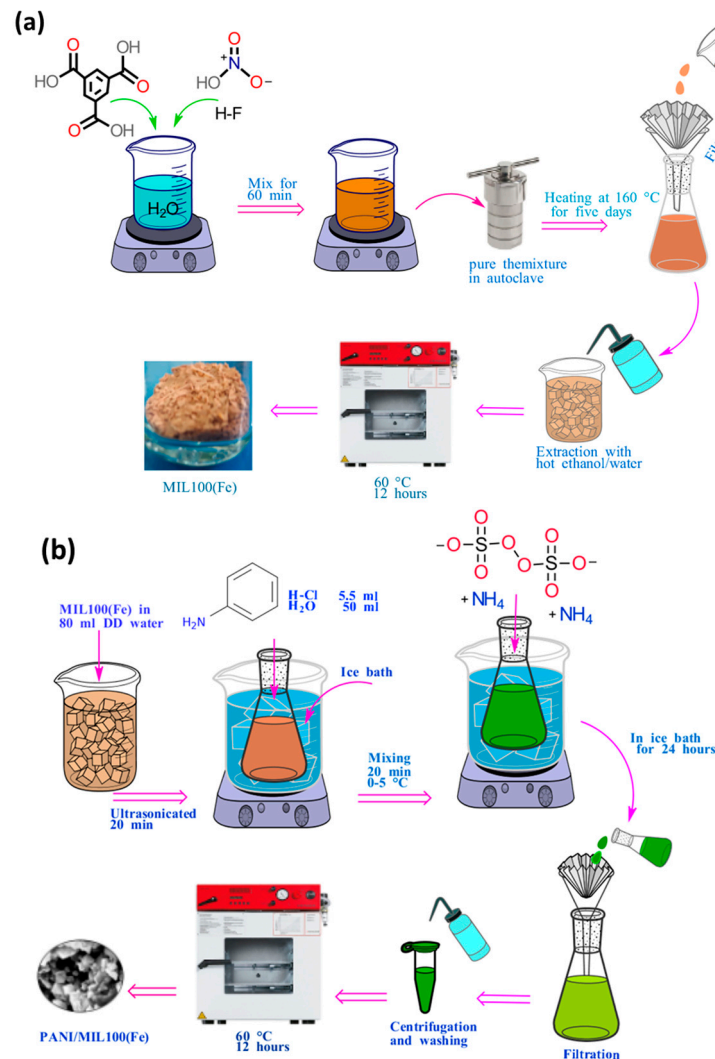


**Figure 1.** The synthesis process of (a) MIL100(Fe) and (b) PANI/MIL100(Fe).

## 2.4. Pb (II) and Cr (VI) Removal Experiments

### 2.4.1. Adsorption Study

To study the sorption performance of Pb (II) and Cr (VI) via the PANI/MIL-100(Fe) adsorbent, firstly a certain concentration of Cr (VI) and Pb (II) aqueous stock solution (200 ppm) was achieved from dissolving a certain amount of Pb(NO<sub>3</sub>)<sub>2</sub> and K<sub>2</sub>Cr<sub>2</sub>O<sub>7</sub> in DD water. The obtained aqueous solutions were also produced at the required concentrations of Cr (VI) and Pb (II) ions. The 0.1 M/0.5 M HCl or NaOH was applied for adjusting the initial pH. The initial and residual Cr (VI) contents were determined by a 2,2'-Diphenylcarbohydrazide method on Ultraviolet–visible (UV-Vis) spectrophotometer (model UNICO 2100, Ridge Road, Suite E Dayton, NJ, USA) at 540 nm wavelength. In this study, a known concentration of stock solution (ranging from 0.0–2.0 ppm) was used to plot the calibration curve [26]. At the end of Pb (II) adsorption, the adsorbent was removed, and residual ion concentrations were determined using an atomic absorption spectrometer (Thermo

Elemental's SOLAAR S Series, Waltham, MA, USA). The removal rate (R) of Cr (VI) and Pb (II) was calculated by Equation (1) [30]:

$$R(\%) = \frac{(C_0 - C_e)}{C_0} \times 100 \quad (1)$$

where  $C_0$  and  $C_e$  show the initial and residual concentration of Cr (VI) and/or Pb (II) ions (ppm), respectively.

#### 2.4.2. Sorption Isotherms, Kinetics, and Thermodynamics Studies

In the isotherm experiments, test solutions (10 mL) of Pb (II) (20–150 ppm) and Cr (VI) (20–50 ppm) were mixed with 10 mg of PANI/MIL-100(Fe). The ion solution's pH was regulated to 2.0 for Cr (VI) and 6.0 for Pb (II), and the experiments were conducted at temperatures of 298, 308, and 318 K consecutively for 120 min. To perform an adsorption kinetics study, 1 mg/mL of PANI/MIL-100(Fe) adsorbent was dispersed in Pb (II) and Cr (VI) solutions with a prearranged initial concentration (pH = 2 for Cr (VI) and pH = 6 for Pb (II)) for dissimilar time intervals (2, 4, 8, 12, 16, 20, 30, 40, 50, 60, 90, and 120 min). At the end of sorption, the concentration of Cr (VI) and Pb (II) ions was analyzed, and the percent uptake ( $q_e$ , mg/g) of metal ions was computed by following Equation (2) [31]:

$$q_e = \frac{(C_0 - C_e)V}{m} \quad (2)$$

where  $q_e$  mentions the magnitude of Cr (VI) or Pb (II) adsorbed per gram of adsorbent at equilibrium (mg/g),  $C_0$  denotes the initial concentration of ions (ppm),  $C_e$  shows the concentration of residual ions (ppm),  $m$  stands for the mass of adsorbent (mg), and  $V$  (mL) refers to the solution volume.

#### 2.4.3. Reusability

Commonly, adsorbent stability in the flow of its reaction is regarded as one of the paramount factors for its practical utility. The reusability test of PANI/MIL-100(Fe) was consummated with 1 mg/mL of the adsorbent immersed in a 20 ppm solution of metal ions at room temperature for 90 min. By the end of each test, the solid precipitate was washed with DD water and dried at 298 K, prepared to be used in the other tests. In this study, 0.1 M NaOH/HCl was applied to regenerate PANI/MIL-100(Fe) adsorbent for Cr (VI) and Pb (II), respectively, after 4 h at 170 rpm followed by separation and washing by DD water [32]. When the first cycle of regeneration was finished, the adsorbents were washed three times with DD water to attain a neutral pH. This adsorption/desorption cycle was reiterated three times.

### 3. Results and Discussions

#### 3.1. Characterization

FT-IR spectrum was performed to describe the material's functional groups (Figure 2). In the IR spectra of PANI/MIL-100(Fe), the broad bands at the zone of 1382–1627  $\text{cm}^{-1}$  are relevant to the existence of symmetrical and asymmetrical stretching vibration of the carboxylate coordinated to metallic ions in the MIL-100(Fe) [33]. The band of 1118  $\text{cm}^{-1}$  is pertinent to the benzene vibration in  $\text{H}_3\text{BTC}$  [28]. Further, as one could observe the peaks with regard to C–H, the C=C groups in benzenoid become obvious at 711 and 758  $\text{cm}^{-1}$  [33,34].

The stretching modes at 1545 and 1468  $\text{cm}^{-1}$  are due to the C=N and C=C for the quinoid and benzenoid rings of PANI, respectively. The mode at 1301  $\text{cm}^{-1}$  is relevant to the C–N in the secondary aromatic amines. As well, the absorption peak of 1240  $\text{cm}^{-1}$  is attributed to the N–H bending vibrations. Finally, a broad band of secondary N–H stretching is assigned at 3440  $\text{cm}^{-1}$  [35].



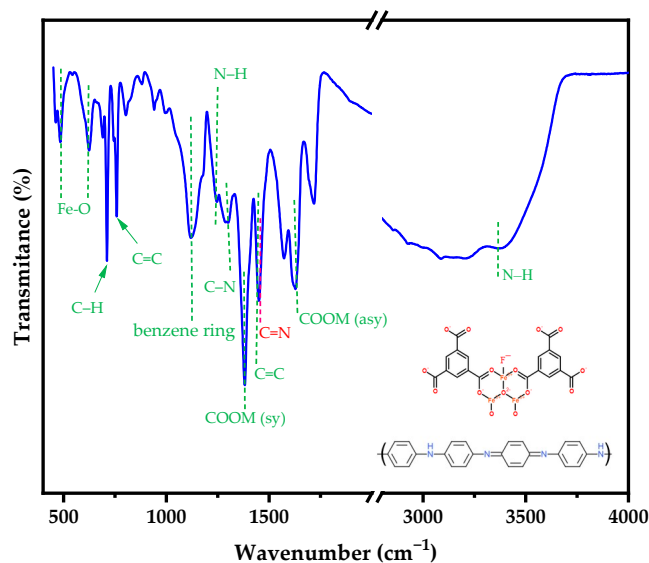


**Figure 2.** FT-IR spectra of PANI/MIL100(Fe).

The structure of samples before and after three successive cycles was recorded using XRD (Figure 3), which indicates no structural transformation occurred. As demonstrated in Figure 3a, the characteristic diffraction peaks at  $2\theta = 11.07^\circ$ ,  $12.63^\circ$ ,  $14.3^\circ$ ,  $20.16^\circ$ ,  $24^\circ$ , and  $27.7^\circ$  were allocated to MIL-100(Fe) in the composite [28]. Moreover, the characteristic bands of PANI were located at  $14.2^\circ$ ,  $20^\circ$ , and  $25.2^\circ$  (Figure 3a), concurring with the (011), (021), and (200) lattice planes [34]. The results support the successful formation of the PANI/MIL-100(Fe).

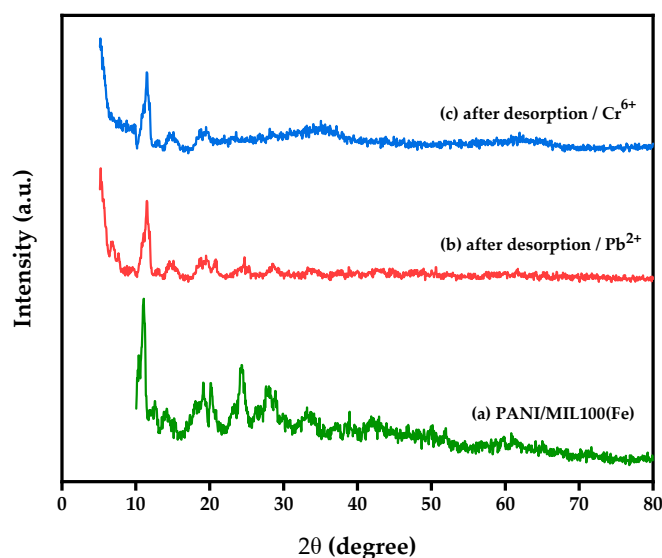


**Figure 3.** X-ray diffractogram of (a) PANI/MIL100(Fe), (b) after desorption of Pb (II), and (c) after Cr (VI) desorption.

Furthermore, XRD patterns for Pb (II) and Cr (VI) ( $2\theta$  of 0 to 80) in the regeneration stage to ensure stability are implied in Figure 3b,c. XRD patterns for PANI/MIL-100(Fe) had no sharp peak from  $2\theta$  of 40 to  $80^\circ$ . The relative intensity of the observed peaks for PANI/MIL-100(Fe) is slightly decreased after treatment with HCl/NaOH as a reagent. Before and after the adsorption, for the case Pb (II), very minor changes were recorded in the crystal structures of the composite. Moreover, the same results were attained for Cr (VI). These facts verify that PANI/MIL-100(Fe) has high stability. To put it another way, the crystal structure of the PANI/MIL-100(Fe) was not affected in the acidic/basic condition.

The SEM picture of the PANI/MIL-100(Fe) was exhibited in Figure 4, which depicted orderly polyhedron or octahedron shapes of MIL-100(Fe). The PANI appeared well-covered onto the surface of MIL-100(Fe) and penetrated the slot of the crystals, which means that most PANI is produced inside the hole of MIL-100(Fe) [36]. It is proven that after the encapsulation of PANI within the framework, even under the acidic prepared condition, the surface structure of the MIL-100(Fe) crystals remains almost intact, which affirms the stability of the MIL-100. Moreover, the stability of the PANI/MIL-100(Fe) was confirmed via XRD patterns after desorption of Cr (VI) and Pb (II) [37].

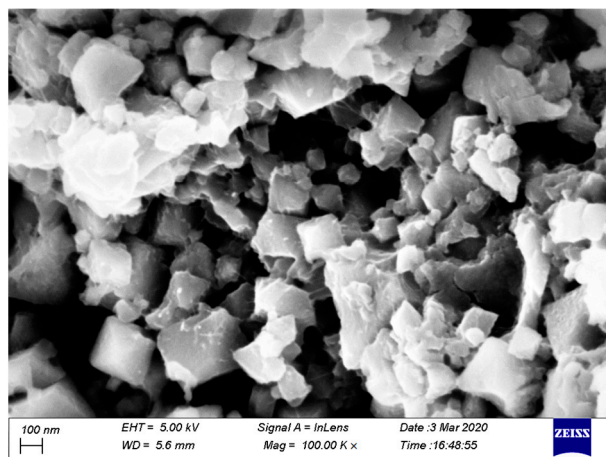


Figure 4. FESEM image of PANI/MIL100(Fe).

Based on the results shown in Figure 5, the  $N_2$  adsorption/desorption of PANI/MIL-100(Fe) exhibited type IV isotherms with microporous distributions. The pore size distribution of the composite was around 1.2 nm. The  $S_{BET}$  and  $S_{Long}$  of the PANI/MIL-100(Fe) were determined to be 159.47 and 261.29  $m^2/g$ , respectively. PANI/MIL-100(Fe) exhibited a much smaller surface area than bulk MIL-100(Fe) ( $S_{BET} = 1843.9 m^2/g$ , our previous work) [28]. This may be owing to the filling of PANI inside the MIL-100(Fe) gaps in the course of the synthesis process. In addition, PANI/MIL-100(Fe) has an amount of 0.2124  $cm^3/g$  for the total pore volume ( $p/p_0 = 0.990$ ), with a magnitude of 5.32 nm for the mean pore diameter.

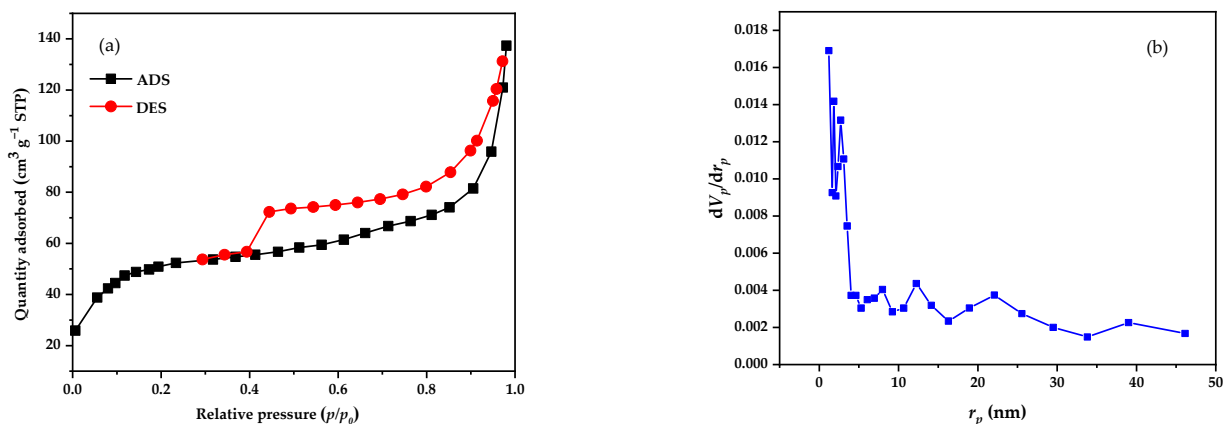
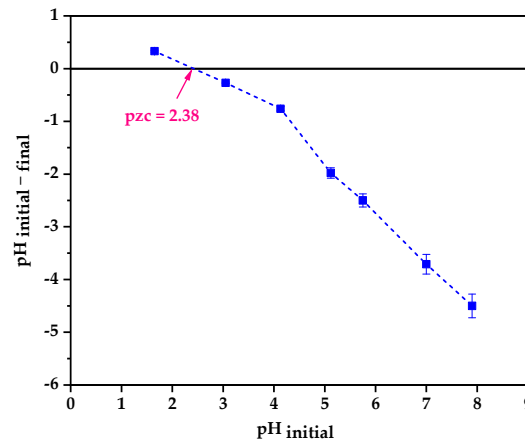


Figure 5. (a)  $N_2$  adsorption–desorption isotherm plot and (b) variations in pore diameter of the PANI/MIL100(Fe) (Desorption, red; Adsorption, black).

### 3.2. pH Influences and Adsorption Mechanism

The point of zero charge, or  $pH_{PZC}$ , is the pH magnitude in which electric charge on the adsorbent's surface is nil.  $pH_{PZC}$  is a vital factor and can help to obtain a better

understanding of the electrostatic interaction between adsorbate molecules with the surface of the adsorbent. The initial pH of solution vs.  $\Delta\text{pH}$  plot for PANI/MIL-100(Fe) is displayed in Figure 6. For this test, 1 mg/mL of the adsorbent was immersed in a solution of NaCl (0.01 M) at room temperature for 48 h [38]. A HCl and NaOH solution (0.01 M) was used to adjust the pH between 2–8. The value of  $\text{pH}_{\text{PZC}}$  achieved was 2.38, which indicated that the pH of  $\sim 2.4$  below the adsorbent surface was positively charged, and above this magnitude the surface charge was negative. Speciation of the adsorbed ions and adsorbent surface chemistry are affected by the solution pH, which in turn can influence the material's sorption features.



**Figure 6.** Determination of  $\text{pH}_{\text{PZC}}$  of PANI/MIL100(Fe).

The effects of pH on the Pb (II) and Cr (VI) adsorption onto PANI/MIL-100(Fe) were assessed over the pH ranging from 2 to 6 (Figure 7). In the acidic condition, Cr (VI) exists as  $\text{HCrO}_4^-$  and  $\text{Cr}_2\text{O}_7^{2-}$  ( $\text{pH} < 5.0$ ), while  $\text{CrO}_4^{2-}$  preponderantly exists at  $\text{pH} > 5.0$ ; accordingly, it can result in significant anions adsorption onto the positively charged surface of the adsorbent via electrostatic attraction. On the contrary, the negatively charged surface groups on the adsorbent at  $\text{pH} > \text{pH}_{\text{PZC}}$  are led to repel the anions in the solution. It can be noted that the Cr (VI) sorption was reduced with rising pH from 2 to 6; consequently, a pH solution of 2 was chosen for the sorption experiments of Cr (VI). For the Pb (II) ion, the equilibrium sorption capacity was bound to be negligible at low pH because of the competitive sorption between  $\text{Pb}^{2+}$  ions and  $\text{H}_3\text{O}^+$ , which enhanced with elevating pH from 2 to 6. In addition, the precipitation of Pb (II) as hydroxides, i.e.,  $\text{Pb}(\text{OH})_3^-$ ,  $\text{Pb}(\text{OH})_2$ , and  $\text{Pb}(\text{OH})^+$ , occurs at  $\text{pH} = 7$ . Hence, a pH solution of 5.5–6 is suggested for examinations of the Pb (II) removal [39].

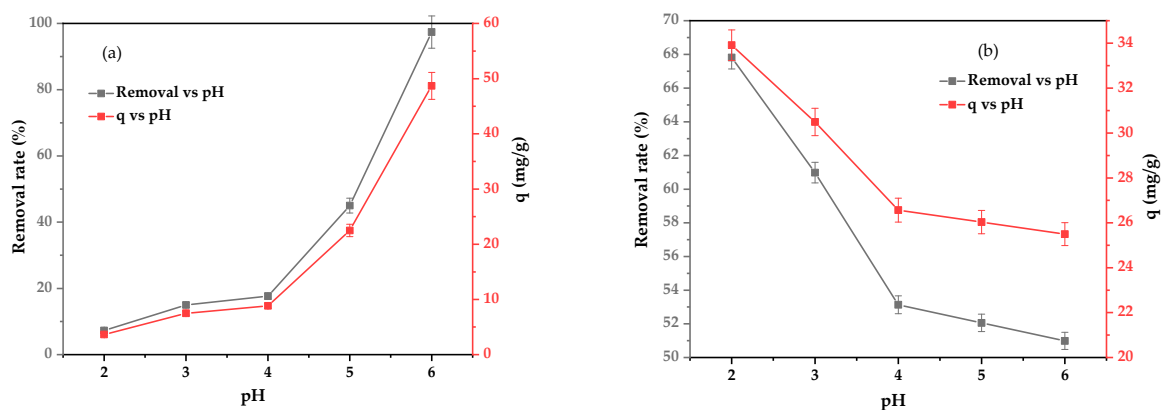


**Figure 7.** Effect of pH value for the adsorption capacity and removal for Pb (II) (a) and Cr (VI) (b) onto PANI/MIL100(Fe), adsorbent dose = 10 mg/10 mL, initial concentration of Cr (VI) = 50 mg/L and  $T = 298\text{ K}$ .



### 3.3. Study of Kinetic Models

In order to study the regulation of Pb (II) and Cr (VI) sorption onto PANI/MIL-100(Fe), pseudo-first and pseudo-second-order models were applied to assess the kinetic information. The kinetic different models, such as pseudo-first-order, pseudo-second-order, and Weber–Morris models (Figures A1–A3), were fitted to the experimental data to investigate the sorption mechanism of Pb (II) and Cr (VI) onto PANI/MIL-100(Fe). Table 1 summarizes the mathematical expression of the kinetic parameters used in this study [40,41].

**Table 1.** Kinetics, isotherms, and other equations used in this study.

Model/Equation	Parameter	Ref
Pseudo-first-order kinetic $\text{Ln}(q_e - q_t) = \text{Ln}q_e - K_1t$	$q_t$ (mg/mL): amount of adsorbate adsorbed at time $t$ $q_e$ (mg/g): equilibrium sorption capacity $K_1$ (1/min): pseudo-first-order equilibrium rate constant	[37]
Pseudo-second-order kinetic $q_t = \frac{q_e^2 K_2 t}{1 + K_2 q_e t}$	$K_2$ (g/mg min): pseudo-second-order equilibrium rate constant	[38]
Intraparticle diffusion $q_t = K_{id}t^{0.5} + C$	$K_{id}$ (mg/g min <sup>1/2</sup> ): intraparticle diffusion rate constant $C$ : boundary layer obtained by extrapolation of the linear portion of the plot of $q_t$ versus $t^{0.5}$	[37]
Langmuir $q_e = \frac{q_{max} K_L C_e}{1 + K_L C_e}$ $R_L = \frac{1}{1 + K_L C_0}$	$q_{max}$ (mg/g): maximum sorption capacity $K_L$ (L/mg): Langmuir sorption equation constant $C_e$ (mg/L): equilibrium adsorbate concentration in solution $C_0$ (mg/L): initial adsorbate concentration in solution $R_L$ : separation factor	[42]
Freundlich $q_e = K_F C_e^{1/n_f}$	$K_F$ (L/mg) <sup>1/n</sup> (mg/g): Freundlich parameter $1/n_f$ : constant corresponded to adsorption intensity	[42]
Temkin $q_e = B_T \text{Ln}(K_T C_e)$ $B_T = \frac{RT}{b_T}$	$K_T$ (L/mg): Temkin adsorption potential $B_T$ (KJ/mol): heat of sorption	[42]
Sips $q_e = \frac{K_s q_{max} C_e^{1/n_s}}{1 + K_s C_e^{1/n_s}}$	$K_s$ (L/mg): Sips model constant $1/n_s$ : Sips model exponent	[25]
$K_c = \frac{C_s}{C_e}$ $\Delta G^\circ = -RT \text{Ln}(K_c)$ $\text{Ln}(K_c) = \frac{\Delta S^\circ}{R} - \frac{\Delta H^\circ}{RT}$	$K_c$ : distribution coefficient $C_s$ (mg/g): amount of ion adsorbent $\Delta G^\circ$ (kJ/mol): change in standard free energy $\Delta S^\circ$ (kJ/mol): standard entropy $\Delta H^\circ$ (kJ/mol): standard enthalpy $R$ (8.314 J/mol K): universal gas constant	[42]
Modified Arrhenius $\theta = \left[1 - \frac{C_e}{C_0}\right]$ $S^* = (1 - \theta)e^{-\left(\frac{E_a}{RT}\right)}$	$E_a$ : activation energy $S^*$ : sticking probability $\theta$ : surface coverage	[35]

The measured kinetic parameters are summarized in Table 2. In a comparative analysis to the pseudo-first-order model, the quantities of  $R^2$  of the pseudo-second-order model are higher and much closer to 1 for both metals. Moreover, for the fitting result of the pseudo-second-order model, it was evident that the  $q_e$  calculated was close to experimental values (for Pb (II):  $q_{e, cal} = 35.40$  mg/g  $q_{e, exp} = 40$  mg/g; for Cr (VI):  $q_{e, cal} = 19.00$  mg/g  $q_{e, exp} = 19.97$  mg/g). According to these finding, the pseudo-second-order model indicates a good description for the sorption of Cr (VI) and Pb (II) onto PANI/MIL-100(Fe) [42].

**Table 2.** Kinetic parameters for Pb (II) and Cr (VI) adsorption at the initial dye concentration of 50 (mg/L) onto MIL-100(Fe)/PANI.

Kinetic Model	Parameters	Pb (II)	Cr (VI)
		50	50
Pseudo-first-order	$K_1$ (1/min)	0.8425	0.3420
	$q_e$ (mg/g)	34.072	17.570
	$R^2$	0.9390	0.8812
Pseudo-second-order	$K_2$ (1/min)	0.0453	0.0246
	$q_e$ (mg/g)	35.408	19.000
	$R^2$	0.9648	0.9575
Intraparticle diffusion	$K_{id,1}$ (mg/g min <sup>1/2</sup> )	1.4887	1.7300
	$C_1$ (mg/g)	26.809	8.8330
	$R^2$	0.9796	0.9040
	$K_{id,2}$ (mg/g min <sup>1/2</sup> )	0.9563	0.6715
	$C_2$ (mg/g)	28.921	13.690
	$R^2$	0.9274	0.8264
	$K_{id,3}$ (mg/g min <sup>1/2</sup> )	1.5188	0.2072
	$C_3$ (mg/g)	24.936	17.780
	$R^2$	0.9110	0.7231

To gain a better understanding of the reaction mechanism, an intraparticle diffusion model (IPD) was utilized. By fitting the data with the IPD model (Figure A3 and Table 2), the adsorption can be divided into three successive linear stages: (1) External mass transfer. In this form, the sorption rate is high, and instantaneous sorption occurs in the first step. Moreover, the mass transfer impetus promotes with the increment of the initial concentration of pollutants, causing a growth of the sorption rate and  $K$  value. (2) Interfacial diffusion is the gradual sorption step, where intraparticle diffusion is controlled. The sorption sites of PANI/MIL-100(Fe) are slowly saturated, the concentration of the solution decreases, and the internal diffusion resistance increases. (3) Intraparticle diffusion. This portion represents the final equilibrium step; the IPD starts to slow down owing to the extremely low solute concentration in solution [43,44].

### 3.4. Experimental Design and Adsorption Isotherms

Isotherm models including the Langmuir, Freundlich, Temkin, and Sips models were used to expose the equilibrium correlation among the concentration of Pb (II) and Cr (VI) ions in solution and the concentration of metal ions retained in the PANI/MIL-100(Fe) at a given temperature. Table 1 summarizes the mathematical expression of isotherms used in this study [28,45].

Nonlinear fitting data for the sorption of Cr (VI) and Pb (II) ions by PANI/MIL-100(Fe) are illustrated in Figures A4 and A5, with detailed fitting parameters summarized in Table 3. Two important factors used to evaluate the fitted model were adjusted: R-Square value ( $R^2$ ) and theoretical maximum sorption capacity ( $q_m$ ). It is obvious that the Sips isotherm with an  $R^2$  magnitude of 0.9953 at a temperature of 318 K for Pb (II) displays the superior results compared with other models. The  $R^2$  of Cr (VI) in various models (Freundlich, Temkin, and Sips) at low temperature, 298 K, was almost the same, indicating that a mixed adsorption mechanism occurred in the sorption process of Cr (VI). In the same vein, the theoretical maximum adsorption capacity ( $q_{max}$ ) for the uptake of Pb (II) and Cr (VI) that was obtained was 81.76 and 72.37 mg/g, respectively. The  $R_L$  magnitudes between 0 and 1; 0.0326, 0.0242, and 0.0173 for Pb (II); and 0.0046, 0.0032, and 0.0023 for Cr (VI) displayed favorable sorption of both two metal ions onto PANI/MIL-100(Fe) at all temperatures.

**Table 3.** Isotherm parameters for Pb (II) and Cr (VI) adsorption onto MIL-100(Fe)/PANI.

Isotherm Parameters	Temperature (K)					
	Pb (II)			Cr (VI)		
	298 K	308 K	318 K	298 K	308 K	318 K
Langmuir						
$q_{\max}$ (mg/g)	67.787	69.103	71.426	39.450	39.515	39.995
$K_L$ (L/mg)	0.3747	0.5088	0.7185	6.1265	8.8427	12.233
$R_L$	0.0326	0.0242	0.0173	0.0046	0.0032	0.0023
$R^2$	0.9552	0.9563	0.9541	0.8437	0.8555	0.9489
Freundlich						
$K_F$ (L/mg) <sup>1/n</sup> (mg/g)	28.113	30.982	33.725	29.325	30.732	32.124
$n_f$	4.6339	4.9407	5.0787	5.7175	6.2932	7.4515
$R^2$	0.8878	0.8860	0.9070	0.9904	0.9794	0.9091
Temkin						
$B_T$ (kJ/mol)	10.591	10.305	10.332	5.325	4.950	4.411
$K_T$ (L/mg)	9.9494	15.632	22.894	301.37	616.43	1803.79
$R^2$	0.9699	0.9719	0.9835	0.9981	0.9979	0.9583
Sips						
$q_{\max}$ (mg/g)	76.934	77.909	81.760	72.370	58.554	43.865
$K_S$ (L/mg)	0.4079	0.5116	0.6183	0.7101	1.203	4.079
$n_s$	1.4799	1.5069	1.6017	3.2154	2.8224	1.6795
$R^2$	0.9879	0.9947	0.9953	0.9965	0.9939	0.9903

In relation to the Freundlich isotherm, the  $K_F$  value obtained 28.11, 30.98, and 33.72 for Pb (II) and 29.32, 30.73, and 32.12 for Cr (VI), respectively. Moreover, all the magnitudes of the Freundlich exponent  $n$  were greater than 1 (Table 3), which depicted that the heterogeneous process is favorable.

The magnitude of  $B_T$  derived from the Temkin isotherm can give information on the chemical or physical nature of the sorption mechanism. In this regard, physisorption mechanisms are reported to have  $B_T$  magnitudes smaller than 20 kJ/mol, whereas the range of 80 to 400 kJ/mol implies chemical sorption [9]. Nevertheless, according to the obtained  $B_T$  values, it can be obviously concluded that a physisorption occurred in the sorption of Cr (VI) and Pb (II) ions on the PANI/MIL-100(Fe) adsorbent. Moreover, based on the equilibrium binding constant, the increase of  $K_T$  values with the rise of temperature reveals that the binding strength between the adsorbate and adsorbent is being strengthened.

In the case of the Sips model,  $q_{\max}$  values were 76.93, 77.90, and 81.76 mg/g for Pb (II) and 72.37, 58.55, and 43.865 mg/g for Cr (VI) at the temperatures of 298, 308, and 318 K, respectively.

### 3.5. Adsorption Thermodynamics

The mathematical expression of thermodynamic factors such as standard Gibb's free energy ( $\Delta G^\circ$ ), enthalpy ( $\Delta H^\circ$ ), entropy change ( $\Delta S^\circ$ ), and activation energy ( $E_a$ ) were summarized in Table 1 [36,43]. The magnitudes of  $\Delta S^\circ$  and  $\Delta H^\circ$  can be estimated by the intercept and slope of a graph of  $\ln(K_c)$  vs.  $1/T$  (Figure 8) [46]. The calculated magnitudes of thermodynamic factors were displayed in Table 4.

All negative magnitudes of the  $\Delta G^\circ$  indicate that the sorption of Cr (VI) and Pb (II) within the PANI/MIL-100(Fe) is spontaneous. When the temperature of the process rises, the absolute magnitudes of Gibb's free energy increase, which shows the degree of spontaneity enhancement. The standard enthalpy magnitudes of Cr (VI) and Pb (II) adsorbed by PANI/MIL-100(Fe) are 17.18 and 32.91 kJ/mol, respectively. According to positive magnitudes of the  $\Delta H^\circ$ , high temperatures are desirable for both metal ions sorption; in other words, results indicated that the sorption mechanism is an endothermic process.

Analogously, all positive magnitudes for the  $\Delta S^\circ$  indicate that the grade of freedom of the sorption system rises with the enhancement of reaction temperature [47].

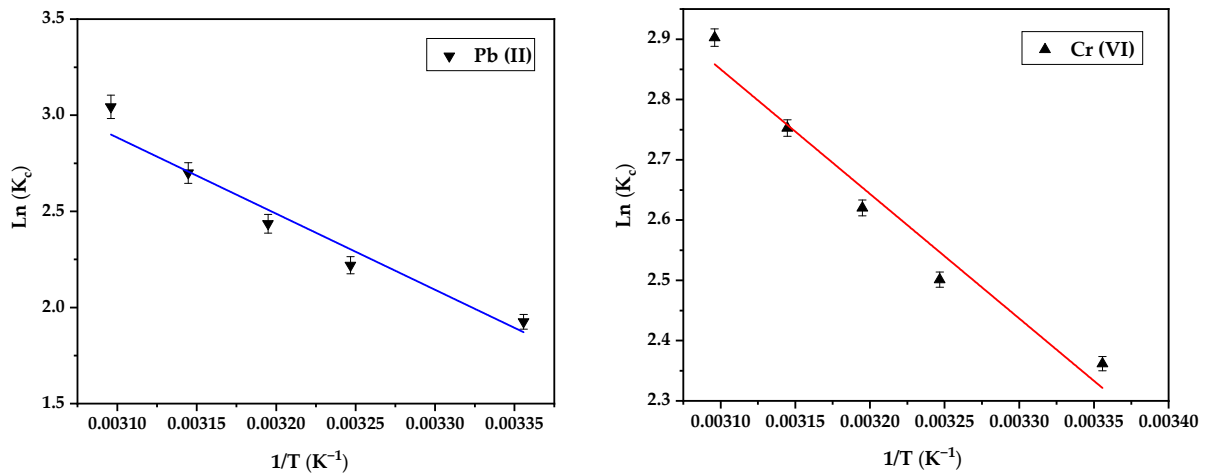


Figure 8. Plots of  $\ln(K_c)$  vs.  $1/T$  for adsorption of Pb (II) and Cr (VI) on PANI/MIL100(Fe).

Table 4. Thermodynamic parameters for the adsorption of Pb (II) and Cr (VI) onto MIL-100(Fe)/PANI.

Heavy Metal Ions	$\Delta G^\circ$ (kJ/mol)					$\Delta H^\circ$ (kJ/mol)	$\Delta S^\circ$ (J/mol·K)	$E_a$ (kJ/mol)
	298 °K	308 °K	313 °K	318 °K	323 °K			
Pb (II)	-4.77167	-5.68388	-6.33805	-7.13721	-8.17302	+32.9148	+126.012	+30.3047
Cr (VI)	-5.85144	-6.40522	-6.81851	-7.27772	-7.79501	+17.1887	+76.9815	+16.0097

Table 4 reported the  $E_a$  defined from the slopes of the straight lines of the modified Arrhenius diagrams from Figure 9. Physisorption and chemisorption are two principal types of adsorptions. Customarily, the range of energies in the physisorption processes is between 5 and 40 kJ/mol, which may be due to the involvement of only weak forces in this process. The rate of chemisorption is affected by temperature, with a limited  $E_a$  in the range of 40–800 kJ/mol [48]. Hence, we can express that the deliberated  $E_a$  is an authentic amount for physisorption. According to the  $E_a$  values, it can be reasoned that the rate-determining stage in the sorption of Cr (VI) and Pb (II) is physisorption, wherein electrons are exchanged between the PANI/MIL-100(Fe) and Pb (II) and Cr (VI).

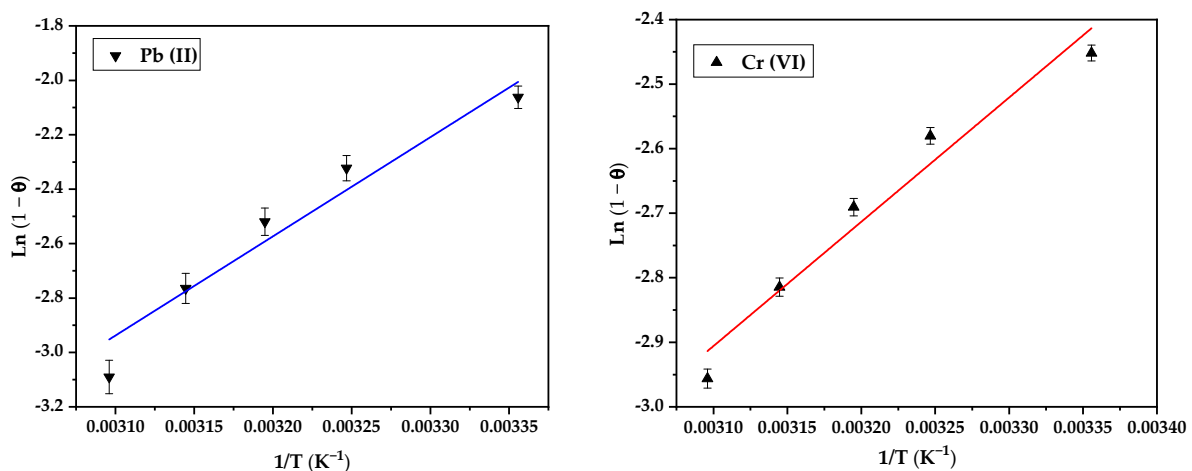
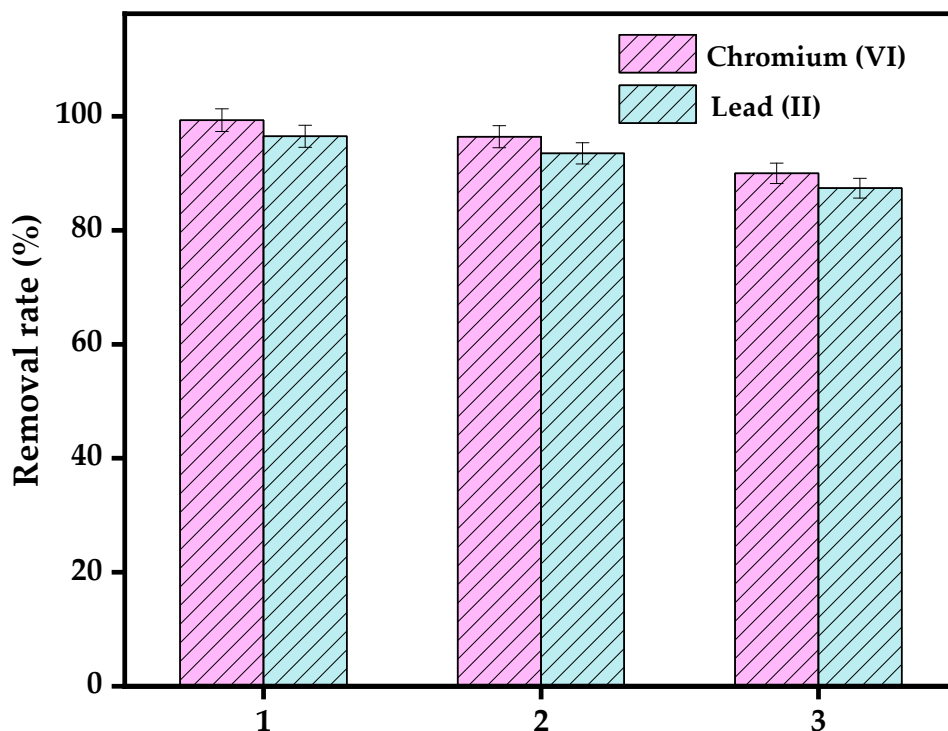


Figure 9. Plots of  $\ln(1 - \theta)$  versus  $1/T$  for adsorption of Pb (II) and Cr (VI) on PANI/MIL100(Fe).

### 3.6. Reusability of the Adsorbent

In order to assay the reuse and recycling properties of the PANI/MIL-100(Fe) (favorable features of a superb adsorbent), reusability analysis was conducted; the results are illustrated in Figure 10. The PANI/MIL-100(Fe) could maintain good sorption uptake after three cycles, still attaining 90% and 87.4% removal for Pb (II) and Cr (VI) after the third recycle. For both metals, the loss of the removal efficiency was nearly 9% after three runs.



**Figure 10.** The performance of PANI/MIL100(Fe) for lead and chromium after three consecutive adsorption/desorption cycles. Error bars represent the standard deviation of the means of three replicates.

### 3.7. Removal Mechanism of Cr (VI) and Pb (II) on PANI/MIL-100(Fe)

The heavy metal ions and PANI/MIL-100(Fe) sorption mechanisms can be imputed in two aspects: one is the sorption capability excited by a large specific surface area; the other is the ion-exchange reaction amid the heavy metal ions and the functional groups on the surface of the adsorbent (Figure 11). Pb (II) sorption using coordination and electrostatic interaction on the surfaces of PANI/MIL-100(Fe) is originated from the presence of C=N (PANI) and  $\text{-COO}^-$  (MIL100) functional groups [28,49]. A key factor of the adsorption mechanism in PANI is the hydrogen atom of the  $\text{-NH-}$  group. In this work, the protonation of ample amine ( $\text{-NH-}$ ) and imine ( $=\text{N-}$ ) groups in the polyaniline chain leads to the production of the  $\text{-NH}^{2+}$  and  $=\text{NH}^+$  acidic sites in the PANI chain, which ultimately can be the active sorption sites for  $\text{HCrO}_4^-$  and  $\text{Cr}_2\text{O}_7^{2-}$ . Hereupon, there exists an acid–base interaction amid the Cr (VI) and the acidic  $\text{-NH}^{2+}$  and  $=\text{NH}^+$  moieties of the MIL-100(Fe)/PANI [46].

The removal mechanism of Pb (II) and Cr (VI) onto PANI/MIL-100(Fe) was examined by FT-IR [47]. According to the FT-IR spectrum, before the adsorption process (Figure 2), it is evident that the  $\text{-NH-}$  modes of PANI/MIL-100(Fe) were at  $1240$  and  $3440\text{ cm}^{-1}$ , and the symmetric stretching of the carboxyl mode was at  $1627\text{ cm}^{-1}$ , while after sorption of heavy metal ions on MIL-100(Fe)/PANI, the locations of all modes shifted impressively (Figure 12). Subsequently, they diminished to  $1127$ ,  $3401$ , and  $1623\text{ cm}^{-1}$  after Cr (VI) was adsorbed and to  $1121$ ,  $3395$ , and  $1621\text{ cm}^{-1}$  after Pb (II) was adsorbed, respectively. This case can be due to the interaction among functional groups on sorbent and metal ions, comprising surface compilations to form metal complexes or electrostatic. Moreover, the



-NH- and carboxyl modes of PANI/MIL-100(Fe) diminished to 1151, 3228, and 1582  $\text{cm}^{-1}$  for Cr (VI) desorption and 1119, 3402, and 1624  $\text{cm}^{-1}$  for Pb (II) desorption.

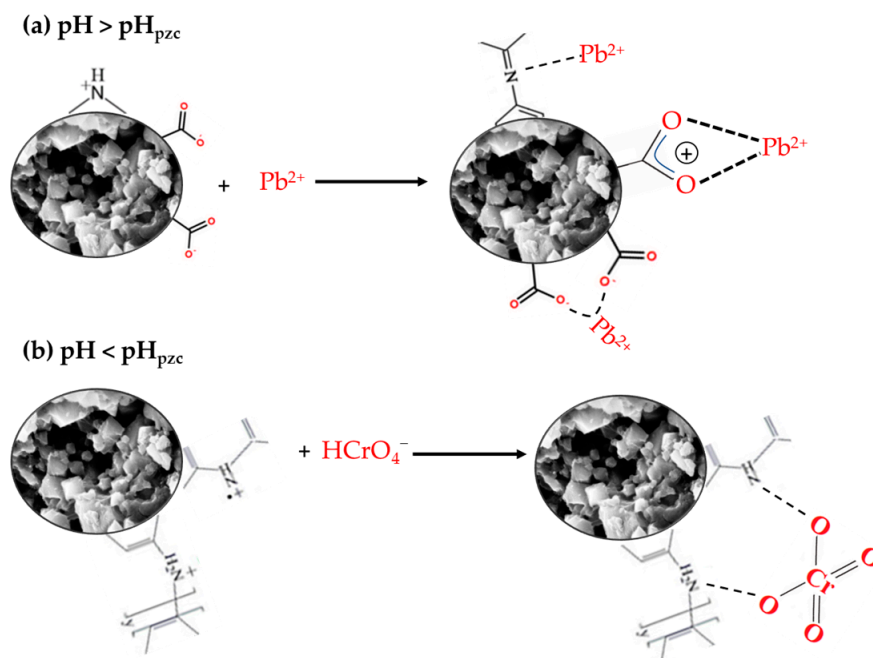


**Figure 11.** Proposed mechanism of (a) Pb (II) and (b) Cr (VI) adsorption onto PANI/MIL-100(Fe): electrostatic attraction and coordination.

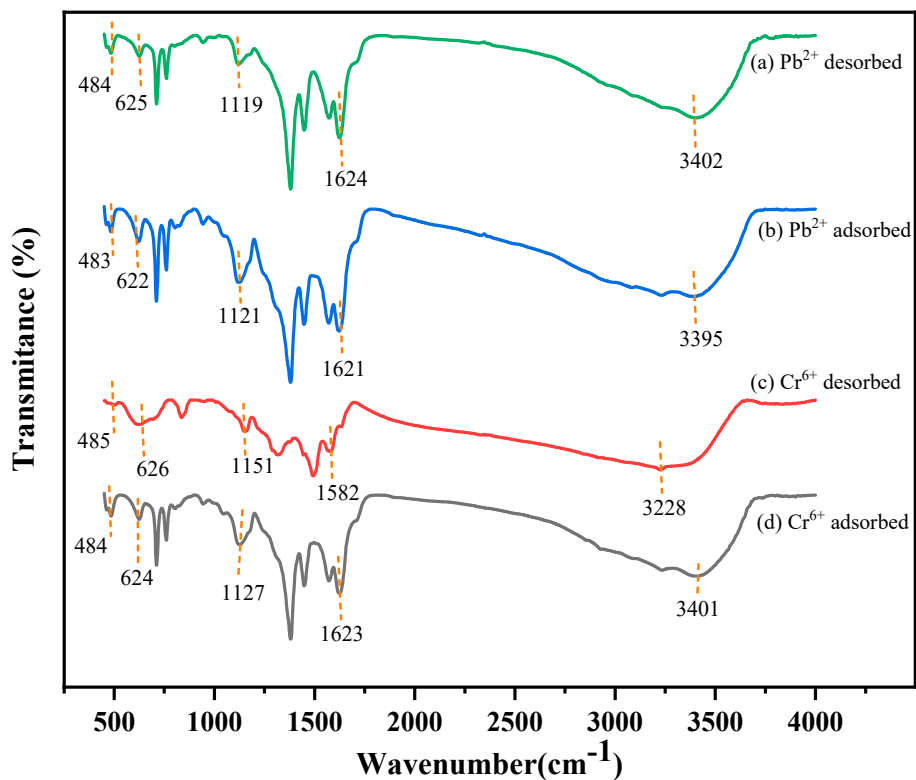


**Figure 12.** FT-IR spectra after Pb (II) desorption (a), after Pb (II) adsorption (b), after Cr (VI) desorption (c), and after Cr (VI) adsorption (d) by PANI/MIL100(Fe) nanocomposite.

Especially, statuses of all peaks after adsorption/desorption changed impressively to lower wavenumbers, indicating that the amine (-NH-) and -COO<sup>-</sup> functional groups had

a great affinity for Pb (II) and Cr (VI), respectively. Moreover, after sorption of heavy metal ions by MIL-100(Fe)/PANI, locations of multiple peaks in the scope of 450–650  $\text{cm}^{-1}$  did not change considerably.

#### 4. Conclusions

A new adsorptive PANI/MIL-100(Fe) material was facily prepared using the hydrothermal method. Firstly, the SEM, BET, XRD, and FT-IR characterizations verified the successful synthesis of PANI/MIL-100(Fe). The functional group and high surface area ( $S_{\text{Long}} = 261.29 \text{ m}^2/\text{g}$ ) of the prepared composite were, respectively, validated using FT-IR and BET analysis. The XRD patterns of PANI/MIL-100(Fe) before and after ion adsorption implied the adsorbent stability in the regeneration step. Furthermore, the obtained PANI/MIL-100(Fe) composite displayed high uptake ability toward Cr (VI) adsorption (72.37 mg/g) and Pb (II) adsorption (81.76 mg/g) at pH = 2 and 6, respectively. The equilibrium and kinetic data of both Pb (II) and Cr (VI) ions adsorption were well-fitted using the Sips isotherm and pseudo-second-order kinetic models that showed the sorption rate dependency upon the availability of the sorption active sites. Furthermore, thermodynamic parameters demonstrated that the sorption mechanism of both Pb (II) and Cr (VI) ions are endothermic, spontaneous, and based on physisorption. The results of the regeneration process showed the high ability of PANI/MIL-100(Fe) adsorbent for both metal ions sorption after three cycles. According to the successful results on the artificial wastewater sample on the removal of target elements, the experimental results will be assessed on the actual wastewater from one of the chemical industries' effluents as a next step.

**Author Contributions:** Conceptualization, A.A., M.F. and L.A.K.; validation, A.A., M.F., and L.A.K.; investigation, A.A., M.F. and L.A.K.; resources, A.A., M.F. and L.A.K.; writing—original draft preparation, A.A., M.F., A.H. and L.A.K.; writing—review and editing, A.A., M.F., A.H. and L.A.K.; visualization, A.A. and A.H.; supervision, A.A. All authors have read and agreed to the published version of the manuscript.

**Funding:** There was no specific funding for this work.

**Data Availability Statement:** Research data can be provided by request.

**Acknowledgments:** The authors gratefully acknowledge the financial and technological support of the Shahrood University of Technology during this research.

**Conflicts of Interest:** The authors declare that they have no known competing financial interest or personal relationships that could have appeared to influence the work reported in this paper.

#### Appendix A

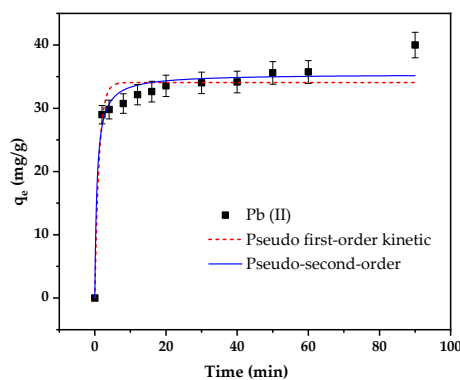


**Figure A1.** Pseudo-first-order kinetic and pseudo-second-order kinetic plot for the adsorption of Pb (II) (conditions: pH 6; dose 10 mg/10 mL; contact time: 90 min; temperature: 298 K).

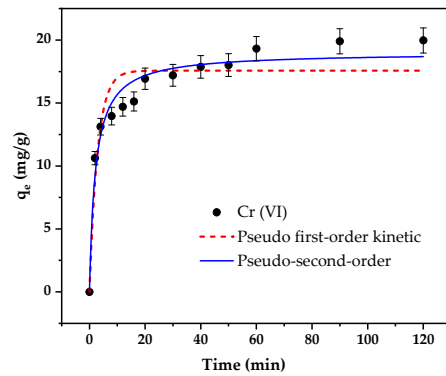


**Figure A2.** Pseudo-first-order kinetic and pseudo-second-order kinetic plot for the adsorption of Cr (VI) (conditions: pH 2; dose 10 mg/10 mL; contact time: 120 min; temperature: 308 K).

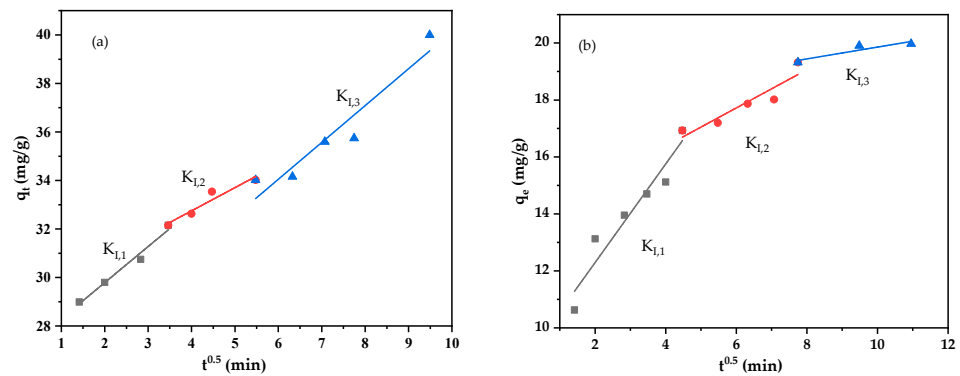


**Figure A3.** Intraparticle diffusion model for the adsorption of Pb (II) (a) and Cr (VI) (b) onto PANI/MIL100(Fe).

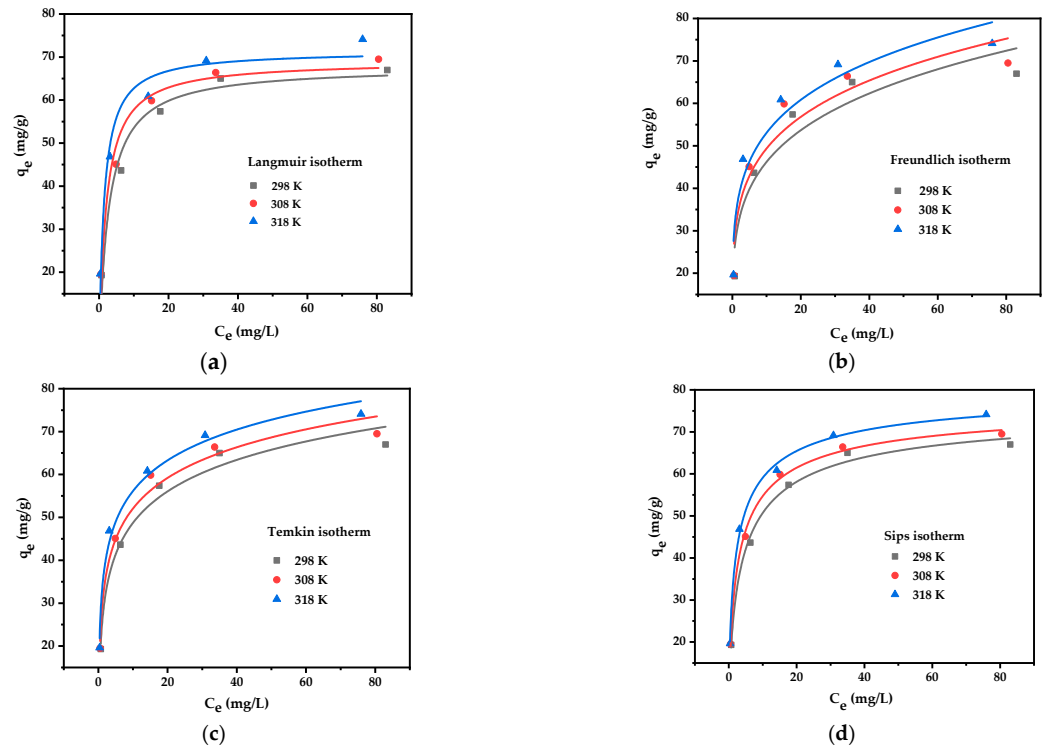


**Figure A4.** (a) Langmuir, (b) Freundlich, (c) Temkin, and (d) Sips adsorption isotherms for Pb (II) removal on PANI/MIL100(Fe).

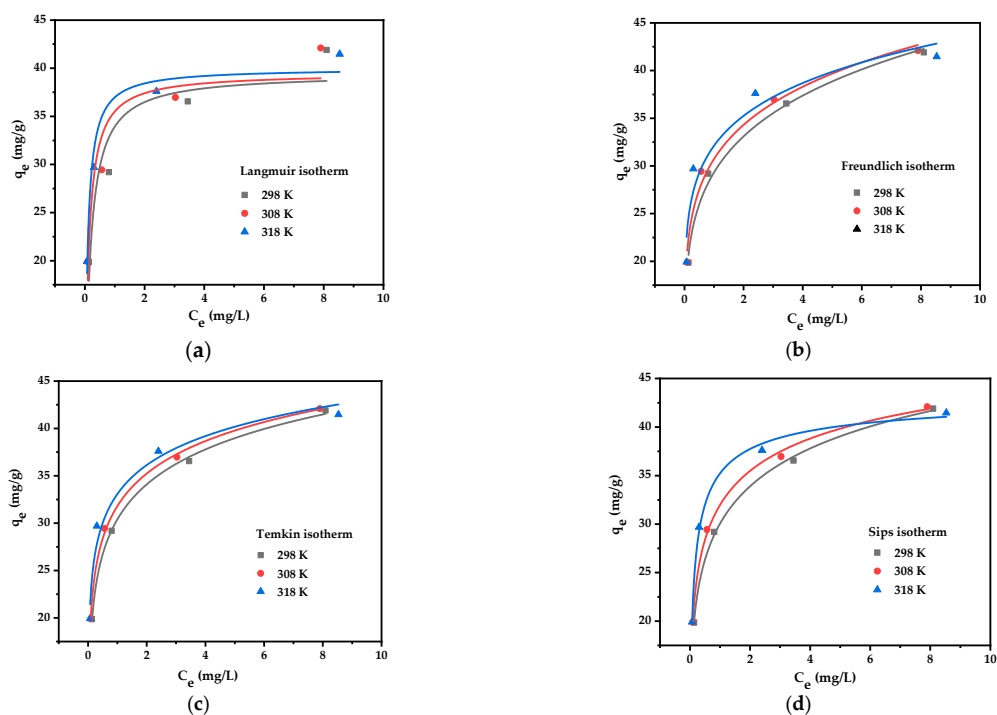


**Figure A5.** (a) Langmuir, (b) Freundlich, (c) Temkin, and (d) Sips adsorption isotherms for Cr (VI) removal on PANI/MIL100(Fe).

## References

- Zare, E.N.; Motahari, A.; Sillanpää, M. Nanoadsorbents based on conducting polymer nanocomposites with main focus on polyaniline and its derivatives for removal of heavy metal ions/dyes: A review. *Environ. Res.* **2018**, *162*, 173–195. [[CrossRef](#)]
- Li, L.-L.; Feng, X.-Q.; Han, R.-P.; Zang, S.-Q.; Yang, G. Cr(VI) removal via anion exchange on a silver-triazolate MOF. *J. Hazard. Mater.* **2017**, *321*, 622–628. [[CrossRef](#)] [[PubMed](#)]
- Thanh, H.; Phuong, T.; Le Hang, P.; Toan, T.; Tuyen, T.; Mau, T.; Khieu, D. Comparative study of Pb (II) adsorption onto MIL-101 and Fe-MIL-101 from aqueous solutions. *J. Environ. Chem. Eng.* **2018**, *6*, 4093–4102. [[CrossRef](#)]
- Thao, V.D.; Giang, B.L.; Thu, T.V. Free-standing polypyrrole/polyaniline composite film fabricated by interfacial polymerization at the vapor/liquid interface for enhanced hexavalent chromium adsorption. *RSC Adv.* **2019**, *9*, 5445–5452. [[CrossRef](#)] [[PubMed](#)]
- Gao, J.; Wu, Z.; Chen, L.; Xu, Z.; Gao, W.; Jia, G.; Yao, Y. Synergistic effects of iron ion and PANI in biochar material for the efficient removal of Cr(VI). *Mater. Lett.* **2019**, *240*, 147–149. [[CrossRef](#)]
- Li, M.; Lv, Z.; Zheng, J.; Hu, J.; Jiang, C.; Ueda, M.; Zhang, X.; Wang, L. Positively Charged Nanofiltration Membrane with Dendritic Surface for Toxic Element Removal. *ACS Sustain. Chem. Eng.* **2017**, *5*, 784–792. [[CrossRef](#)]
- Bulut, Y.; Tez, Z. Removal of heavy metals from aqueous solution by sawdust adsorption. *J. Environ. Sci.* **2007**, *19*, 160–166. [[CrossRef](#)]
- Liu, Z.; Chen, J.; Wu, Y.; Li, Y.; Zhao, J.; Na, P. Synthesis of magnetic orderly mesoporous  $\alpha$ -Fe<sub>2</sub>O<sub>3</sub> nanocluster derived from MIL-100(Fe) for rapid and efficient arsenic (III,V) removal. *J. Hazard. Mater.* **2018**, *343*, 304–314. [[CrossRef](#)]
- Kheshtzar, I.; Ghorbani, M.; Gatabi, M.; Lashkenari, M. Facile synthesis of smartaminosilane modified-SnO<sub>2</sub>/porous silica nanocomposite for high efficiency removal of lead ions and bacterial inactivation. *J. Hazard. Mater.* **2018**, *359*, 19–30. [[CrossRef](#)]
- Jiménez-Rodríguez, A.; Durán-Barrantes, M.; Borja, R.; Sánchez, E.; Colmenarejo, M.; Raposo, F. Heavy metals removal from acid mine drainage water using biogenic hydrogen sulphide and effluent from anaerobic treatment: Effect of pH. *J. Hazard. Mater.* **2009**, *165*, 759–765. [[CrossRef](#)]
- Yaghi, O.M.; Li, H. Hydrothermal Synthesis of a Metal-Organic Framework Containing Large Rectangular Channels. *J. Am. Chem. Soc.* **1995**, *117*, 10401–10402. [[CrossRef](#)]
- Zheng, X.; Wang, J.; Xue, X.; Liu, W.; Kong, Y.; Cheng, R.; Yuan, D. Facile synthesis of Fe<sub>3</sub>O<sub>4</sub>@MOF-100(Fe) magnetic microspheres for the adsorption of diclofenac sodium in aqueous solution. *Environ. Sci. Pollut. Res.* **2018**, *25*, 31705–31717. [[CrossRef](#)] [[PubMed](#)]
- Zhou, L.; Li, N.; Jin, X.; Owens, G.; Chen, Z. A new nFe@ZIF-8 for the removal of Pb (II) from wastewater by selective adsorption and reduction. *J. Colloid Interface Sci.* **2020**, *565*, 167–176. [[CrossRef](#)] [[PubMed](#)]
- Zhang, H.; Wen, J.; Fang, Y.; Zhang, S.; Zeng, G. Influence of fulvic acid on Pb(II) removal from water using a post-synthetically modified MIL-100(Fe). *J. Colloid Interface Sci.* **2019**, *551*, 155–163. [[CrossRef](#)]
- Herath, A.; Navarathna, C.; Warren, S.; Perez, F.; Pittman, C.P., Jr.; Mlsna, T. Iron/titanium oxide-biochar (Fe<sub>2</sub>TiO<sub>5</sub>/BC): A versatile adsorbent/photocatalyst for aqueous Cr (VI), Pb<sup>2+</sup>, F- and methylene blue. *J. Colloid Interface Sci.* **2022**, *614*, 603–616. [[CrossRef](#)]

16. Babaei, M.; Salehi, S.; Anbia, M.; Kazemipour, M. Improving CO<sub>2</sub> adsorption capacity and CO<sub>2</sub>/CH<sub>4</sub> selectivity with amine functionalization of MIL-100 and MIL-101. *J. Chem. Eng. Data* **2018**, *63*, 1657–1662. [[CrossRef](#)]
17. Xu, F.; Sun, L.; Huang, P.; Sun, Y.; Zheng, Q.; Zou, Y.; Chu, H.; Yan, E.; Zhang, H.; Wang, J.; et al. A pyridine vapor sensor based on metal-organic framework-modified quartz crystal microbalance. *Sens. Actuators B Chem.* **2018**, *254*, 872–877. [[CrossRef](#)]
18. Kent, C.A.; Liu, D.; Meyer, T.J.; Lin, W. Amplified Luminescence Quenching of Phosphorescent Metal-Organic Frameworks. *J. Am. Chem. Soc.* **2012**, *134*, 3991–3994. [[CrossRef](#)]
19. Sepehrmansouri, H.; Zarei, M.; Zolfigol, M.A.; Moosavi-Zare, A.R.; Rostamnia, S.; Moradi, S. Multilinker phosphorous acid anchored En/MIL-100(Cr) as a novel nanoporous catalyst for the synthesis of new N-heterocyclic pyrimido [4,5-b] quinolines. *Mol. Catal.* **2020**, *481*, 110303. [[CrossRef](#)]
20. Strzemppek, W.; Menezek, E.; Gil, B. Fe-MIL-100 as drug delivery system for asthma and chronic obstructive pulmonary disease treatment and diagnosis. *Microporous Mesoporous Mater.* **2019**, *280*, 264–270. [[CrossRef](#)]
21. Zhang, B.-L.; Qiu, W.; Wang, P.-P.; Liu, Y.-L.; Zou, J.; Wang, L.; Ma, J. Mechanism study about the adsorption of Pb(II) and Cd(II) with iron-trimesic metal-organic frameworks. *Chem. Eng. J.* **2020**, *385*, 123507. [[CrossRef](#)]
22. Rahimi, E.; Mohaghegh, N. Removal of Toxic Metal Ions from Sungun Acid Rock Drainage Using Mordenite Zeolite, Graphene Nanosheets, and a Novel Metal-Organic Framework. *Mine Water Environ.* **2016**, *35*, 18–28. [[CrossRef](#)]
23. Khan, N.A.; Yoo, D.K.; Jhung, S.H. Polyaniline-Encapsulated Metal-Organic Framework MIL-101: Adsorbent with Record-High Adsorption Capacity for the Removal of Both Basic Quinoline and Neutral Indole from Liquid Fuel. *ACS Appl. Mater. Interfaces* **2018**, *10*, 35639–35646. [[CrossRef](#)] [[PubMed](#)]
24. Lakouraj, M.; Zare, E.; Moghadam, P. Synthesis of novel conductive poly (p-phenylenediamine)/Fe<sub>3</sub>O<sub>4</sub> nanocomposite via emulsion polymerization and investigation of antioxidant activity. *Adv. Polym. Technol.* **2014**, *33*. [[CrossRef](#)]
25. Karthik, R.; Meenakshi, S. Removal of Pb(II) and Cd(II) ions from aqueous solution using polyaniline grafted chitosan. *Chem. Eng. J.* **2015**, *263*, 168–177. [[CrossRef](#)]
26. Jiang, Y.; Liu, Z.; Zeng, G.; Liu, Y.; Shao, B.; Li, Z.; Liu, Y.; Zhang, W.; He, Q. Polyaniline-based adsorbents for removal of hexavalent chromium from aqueous solution: A mini review. *Environ. Sci. Pollut. Res.* **2018**, *25*, 6158–6174. [[CrossRef](#)]
27. Bushra, R.; Shahadat, M.; Raeissi, A.; Nabi, S.A. Development of nano-composite adsorbent for removal of heavy metals from industrial effluent and synthetic mixtures; its conducting behavior. *Desalination* **2012**, *289*, 1–11. [[CrossRef](#)]
28. Forghani, M.; Azizi, A.; Livani, M.; Kafshgari, L. Adsorption of lead (II) and chromium (VI) from aqueous environment onto metal-organic framework MIL-100(Fe): Synthesis, kinetics, equilibrium and thermodynamics. *J. Solid State Chem.* **2020**, *291*, 121636. [[CrossRef](#)]
29. Chen, D.-D.; Yi, X.-H.; Zhao, C.; Fu, H.; Wang, P.; Wang, C.-C. Polyaniline modified MIL-100(Fe) for enhanced photocatalytic Cr(VI) reduction and tetracycline degradation under white light. *Chemosphere* **2020**, *245*, 125659. [[CrossRef](#)]
30. Poudel, M.B.; Awasthi, G.P.; Kim, H.J. Novel insight into the adsorption of Cr(VI) and Pb(II) ions by MOF derived Co-Al layered double hydroxide @hematite nanorods on 3D porous carbon nanofiber network. *Chem. Eng. J.* **2021**, *417*, 129312. [[CrossRef](#)]
31. Kharrazi, S.M.; Soleimani, M.; Jokar, M.; Richards, T.; Pettersson, A.; Mirghaffari, N. Pretreatment of lignocellulosic waste as a precursor for synthesis of high porous activated carbon and its application for Pb (II) and Cr (VI) adsorption from aqueous solutions. *Int. J. Biol. Macromol.* **2021**, *180*, 299–310. [[CrossRef](#)] [[PubMed](#)]
32. Fang, Y.; Wen, J.; Zeng, G.; Jia, F.; Zhang, S.; Peng, Z.; Zhang, H. Effect of mineralizing agents on the adsorption performance of metal-organic framework MIL-100(Fe) towards chromium (VI). *Chem. Eng. J.* **2018**, *337*, 532–540. [[CrossRef](#)]
33. Karami, K.; Beram, S.M.; Siadatnasab, F.; Bayat, P.; Ramezanzpour, A. An investigation on MIL-101 Fe/PANI/Pd nanohybrid as a novel photocatalyst based on MIL-101(Fe) metal-organic frameworks removing methylene blue dye. *J. Mol. Struct.* **2021**, *1231*, 130007. [[CrossRef](#)]
34. Zhang, Y.; Jiang, D.; Wang, Y.; Zhang, T.; Xiang, G.; Zhang, Y.-X.; Yuan, S. Core-shell structured magnetic  $\gamma$ -Fe<sub>2</sub>O<sub>3</sub>@ PANI nanocomposites for enhanced As (V) adsorption. *Ind. Eng. Chem. Res.* **2020**, *59*, 7554–7563. [[CrossRef](#)]
35. Seo, Y.-K.; Chitale, S.K.; Lee, U.-H.; Patil, P.; Chang, J.-S.; Hwang, Y.K. Formation of Polyaniline-MOF Nanocomposites Using Nano-Sized Fe(III)-MOF for Humidity Sensing Application. *J. Nanosci. Nanotechnol.* **2019**, *19*, 8157–8162. [[CrossRef](#)]
36. An, J.; Li, Y.; Chen, W.; Li, G.; He, J.; Feng, H. Electrochemically-deposited PANI on iron mesh-based metal-organic framework with enhanced visible-light response towards elimination of thiamphenicol and E. coli. *Environ. Res.* **2020**, *191*, 110067. [[CrossRef](#)]
37. Kameda, T.; Honda, R.; Kumagai, S.; Saito, Y.; Yoshioka, T. Adsorption of Cu<sup>2+</sup> and Ni<sup>2+</sup> by tripolyphosphate-crosslinked chitosan-modified montmorillonite. *J. Solid State Chem.* **2019**, *277*, 143–148. [[CrossRef](#)]
38. Kafshgari, L.; Ghorbani, M.; Azizi, A. Fabrication and investigation of MnFe<sub>2</sub>O<sub>4</sub>/MWCNTs nanocomposite by hydrothermal technique and adsorption of cationic and anionic dyes. *Appl. Surf. Sci.* **2017**, *419*, 70–83. [[CrossRef](#)]
39. Mishra, S.; Yadav, A.; Verma, N. Carbon gel-supported Fe-graphene disks: Synthesis, adsorption of aqueous Cr (VI) and Pb (II) and the removal mechanism. *Chem. Eng. J.* **2017**, *326*, 987–999. [[CrossRef](#)]
40. Kim, Y.-S.; Kim, J.-H. Isotherm, kinetic and thermodynamic studies on the adsorption of paclitaxel onto Sylopute. *J. Chem. Thermodyn.* **2019**, *130*, 104–113. [[CrossRef](#)]
41. Uthayakumar, H.; Radhakrishnan, P.; Shanmugam, K.; Kushwaha, O.S. Growth of MWCNTs from Azadirachta indica oil for optimization of chromium(VI) removal efficiency using machine learning approach. *Environ. Sci. Pollut. Res.* **2022**, *29*, 34841–34860. [[CrossRef](#)] [[PubMed](#)]



42. Touihri, M.; Guesmi, F.; Hannachi, C.; Hamrouni, B.; Sellaoui, L.; Badawi, M.; Poch, J.; Fiol, N. Single and simultaneous adsorption of Cr (VI) and Cu (II) on a novel Fe<sub>3</sub>O<sub>4</sub>/pine cones gel beads nanocomposite: Experiments, characterization and isotherms modeling. *Chem. Eng. J.* **2021**, *416*, 129101. [[CrossRef](#)]
43. Li, S.; Ma, R.; Zhu, X.; Liu, C.; Li, L.; Yu, Z.; Chen, X.; Li, Z.; Yang, Y. Sorption of tetrabromobisphenol A onto microplastics: Behavior, mechanisms, and the effects of sorbent and environmental factors. *Ecotoxicol. Environ. Saf.* **2021**, *210*, 111842. [[CrossRef](#)] [[PubMed](#)]
44. Wu, F.-C.; Tseng, R.-L.; Juang, R.-S. Initial behavior of intraparticle diffusion model used in the description of adsorption kinetics. *Chem. Eng. J.* **2009**, *153*, 1–8. [[CrossRef](#)]
45. Babapour, M.; Dehghani, M.; Alimohammadi, M.; Arjmand, M.; Salari, M.; Rasuli, L.; Mubarak, N.; Khan, N. Adsorption of Cr (VI) from aqueous solution using mesoporous metal-organic framework-5 functionalized with the amino acids: Characterization, optimization, linear and nonlinear kinetic models. *J. Mol. Liq.* **2022**, *345*, 117835. [[CrossRef](#)]
46. Lai, Y.; Wang, F.; Zhang, Y.; Ou, P.; Wu, P.; Fang, Q.; Chen, Z.; Li, S. UiO-66 derived N-doped carbon nanoparticles coated by PANI for simultaneous adsorption and reduction of hexavalent chromium from waste water. *Chem. Eng. J.* **2019**, *378*, 122069. [[CrossRef](#)]
47. Zhang, Z.; Wang, T.; Zhang, H.; Liu, Y.; Xing, B. Adsorption of Pb (II) and Cd (II) by magnetic activated carbon and its mechanism. *Sci. Total Environ.* **2021**, *757*, 143910. [[CrossRef](#)]
48. Shikuku, V.O.; Zanella, R.; Kowenje, C.O.; Donato, F.F.; Bandeira, N.M.G.; Prestes, O.D. Single and binary adsorption of sulfonamide antibiotics onto iron-modified clay: Linear and nonlinear isotherms, kinetics, thermodynamics, and mechanistic studies. *Appl. Water Sci.* **2018**, *8*, 175. [[CrossRef](#)]
49. Wang, H.; Wang, S.; Wang, S.; Tang, J.; Chen, Y.; Zhang, L. Adenosine-functionalized UiO-66-NH<sub>2</sub> to efficiently remove Pb (II) and Cr (VI) from aqueous solution: Thermodynamics, kinetics and isothermal adsorption. *J. Hazard. Mater.* **2022**, *425*, 127771. [[CrossRef](#)]

**Disclaimer/Publisher's Note:** The statements, opinions and data contained in all publications are solely those of the individual author(s) and contributor(s) and not of MDPI and/or the editor(s). MDPI and/or the editor(s) disclaim responsibility for any injury to people or property resulting from any ideas, methods, instructions or products referred to in the content.